

Geochronology and geochemistry of the Dasuji Mo deposit in the northern margin of the North China Block: Implications for ore genesis and tectonic setting

Yong Zhang^{a,*}, Yu-Bo Ma^a, Tong Zhang^b, Zeng-Jie Zhang^a, Jian-Hua Ding^a, Chao Li^c

^a MNR Key Laboratory of Metallogeny and Mineral Assessment, Institute of Mineral Resources, Chinese Academy of Geological Sciences, Beijing 100037, China

^b Geological Survey Institute of Inner Mongolia, Hohhot 010020, China

^c National Research Center for Geoanalysis, Beijing 100037, China

ARTICLE INFO

Keywords:
Geochronology
Sr–Nd–Hf isotopes
Porphyry Mo deposit
Dasuji
North China Block

ABSTRACT

The Dasuji Mo deposit is located in the northern margin of the North China Block (NCB). In this paper, we present the whole-rock major and trace elements and the Sr–Nd isotopic data, zircon U–Pb and Hf isotopic data, and molybdenite Re–Os data for the units associated with the deposit. Laser ablation inductively coupled plasma mass spectrometry (LA–ICP–MS) dating of zircons from the granite porphyry yielded an age of 220.3 ± 0.7 Ma, which was interpreted to be the emplacement age of this intrusion. The molybdenite Re–Os dating yielded model ages of 219.9–217.4 Ma, an isochron age of 222.1 ± 4.7 Ma, and a weighted mean model age of 218.9 ± 1.6 Ma, representing the timing of the formation of the Mo mineralization. The Dasuji granite porphyry contains high-K calc-alkaline and peraluminous rocks and is characterized by relatively high LREEs and low HREEs; depleted Ba, Sr, P and Ti; and negative Eu anomalies and are of highly fractionated I-type granitoids. The whole-rock ϵ Nd(t) and zircon ϵ Hf(t) values for the granite porphyry range from -13.9 to -12.8 and -16.4 to -7.3 , respectively, indicating that the magma was generated by the partial melting of ancient lower crust materials. The Dasuji Mo deposit may have formed in a post-collisional extensional setting.

1. Introduction

The North China Block (NCB) is one of the oldest cratons in the world (Fig. 1a, Liu et al., 1992; Zheng et al., 2013), and experienced a very complicated evolutionary history of geological events (Zhai, 2010; Zhai and Santosh, 2013; Yang and Santosh, 2017). Metallogenesis was closely related to the major geological events, and the multiple geological events recorded in this area generated significant numbers of mineral deposits, making this region one of the most important areas in the polymetallic metallogenic belt in China for REEs, Mo, Pb, Zn, and Au (Zhai, 2010; Zhang et al., 2016a). Five episodes of mineralization are recognized in this region (Zhai and Santosh, 2013): late Neoarchean, Paleoproterozoic, Mesoproterozoic, Paleozoic and Mesozoic. As an important metallogenic belt, the abundant deposits have been the focus of many studies, especially the numerous new discoveries of Mo deposits (Zhang et al., 2010a; Zeng et al., 2011a, 2012a, 2013a; Chen et al., 2012, 2016; Shu et al., 2014, 2015, 2016; Wu et al., 2017).

This study focuses on central Inner Mongolia, which is located within the NCB and is an area that contains numerous Au, Pb, Zn, and Mo deposits (Fig. 2); recent discoveries in this area include the giant sized Caosiya and the large sized Dasuji Mo deposits. The Dasuji Mo deposit is located in the central segment of the northern margin of the NCB and was discovered and delineated during the 2000s. Previous research has focused on the geology, and geochronology of the deposit (Yu et al., 2008; Zhang et al., 2009a; Li, 2012; Nie et al., 2012; Wu, 2015). However, the mineralization age and the ore-related intrusions remain unclear. The mineralization formed during the Yanshanian (Yu et al., 2008; Li, 2012) and Indosian periods (Zhang et al., 2009a; Wu, 2015); the ore-related intrusions are syenogranite (Li, 2012), syenogranite and quartz porphyry (Yu et al., 2008), and granite porphyry (Wu, 2015). To understand the metallogenesis of the Mo deposit and its genetic relationship to the host granites, we present new geological, zircon U–Pb and molybdenite Re–Os geochronological, geochemical, and Sr, Nd, and Hf isotopic data for the granite porphyry associated with the Dasuji Mo deposit. Combined with previously published data,

* Corresponding author at: MNR Key Laboratory of Metallogeny and Mineral Assessment, Institute of Mineral Resources, Chinese Academy of Geological Sciences, Beijing 100037, China.

E-mail address: zyong@cags.ac.cn (Y. Zhang).

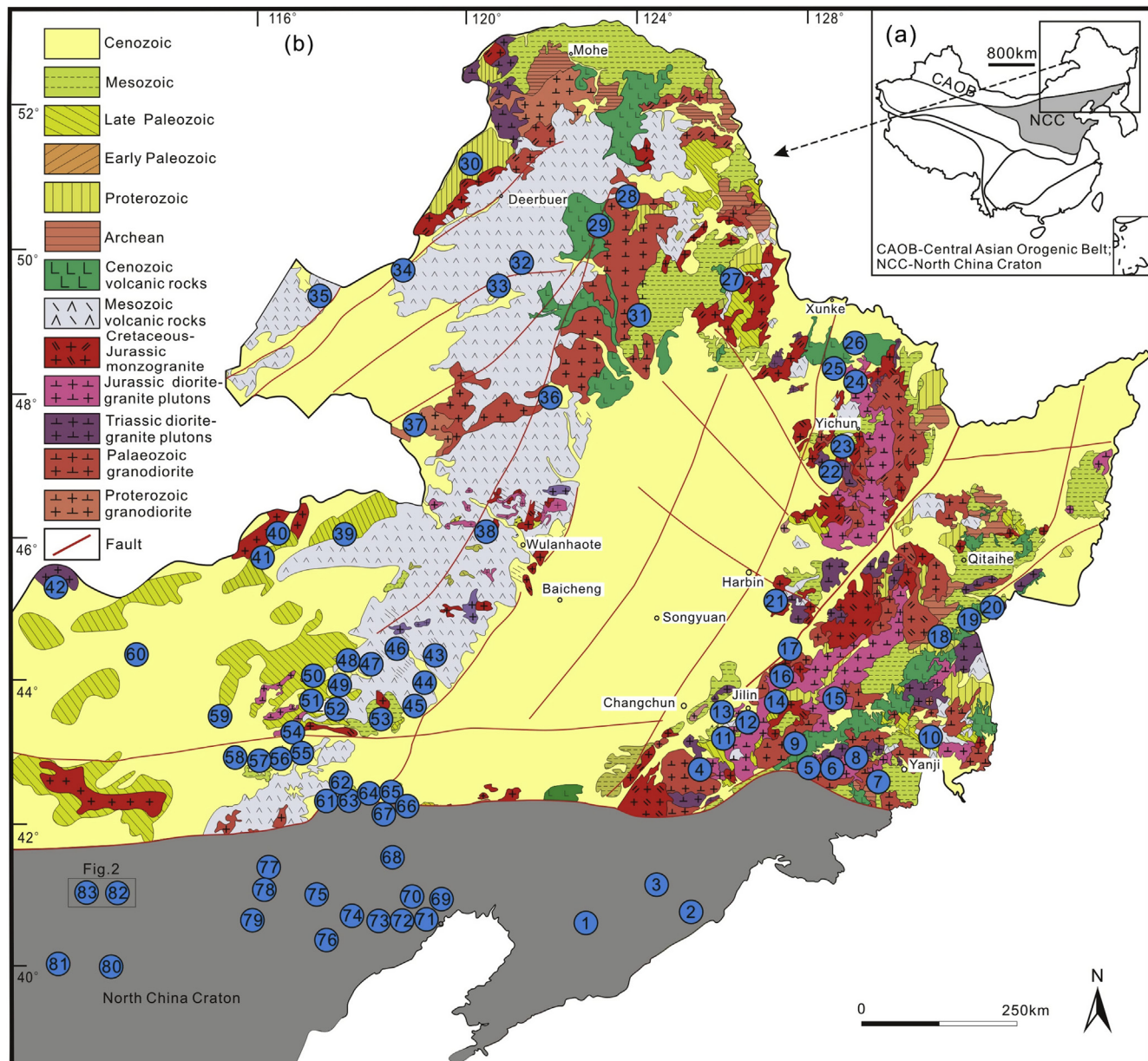


Fig. 1. Sketch geological map of northeast China showing the distribution of the Mo deposits and their associated granitoids. The data sources and deposit numbers are listed in [Supplementary Table 1](#).

we use these data to determine the Mo mineralization and granite porphyry formation ages in this area and to elucidate the characteristics of the source region for the magmas, petrogenesis, and tectonic setting.

2. Geological setting

The study area is located in the central segment of the northern margin of the NCB, which has experienced multiple stages of tectonism and magmatism. Five major tectonic events are recognized in this region (Zhai, 2010; Zhai and Santosh, 2011, 2013; Santosh et al., 2012, 2013; Zheng et al., 2013; Qiu et al., 2016; Wu et al., 2018): Neoarchean crustal growth and stabilization, Paleoproterozoic rifting–subduction–accretion–collision, and late Paleoproterozoic–Neoproterozoic multistage rifting. From the Paleozoic to the Mesozoic, this area was significantly affected by the evolution and final closure of the Paleo-Asian Ocean. After the closure of the Paleo-Asian Ocean, this area was overprinted and modified during the subduction of the Pacific Plate (Xiao et al., 2003; Miao et al., 2008; Wu et al., 2011; Meng et al., 2011;

Xu et al., 2013). This tectonic complexity, combined with the multiple stages of tectonism and magmatism, makes this region well-endowed with large-scale endogenic mineralization. The exposed strata in our study area are mainly the Paleoarchean Xinghe Group, Mesoarchean Jining Group, Neoarchean Seertengshan Group, Palaeoproterozoic Erdaoao Group, and Proterozoic, Paleozoic, Mesozoic, and Cenozoic strata (Inner Mongolia Autonomous Region Bureau of Geology and Mineral Resource, 1991). The structure of the area is dominated by the E-W-trending Guyang–Wuchuang–Shangyi, and the NEE-trending Linhe–Baotou–Hohhot–Jining faults. The intrusions contain tonalite, granite porphyry, quartz porphyry, and syenogranite-porphyry.

3. Geology of the Dasuji Mo deposit

The Dasuji Mo deposit is located 26 km southeast of Zhuozi County, Inner Mongolia; it is a large porphyry Mo deposit containing 149,358 tons of Mo at 0.03%–0.30% grade (Zhang et al., 2009a; Wu, 2015). The exposed strata in the Dasuji Mo deposit is dominated by the

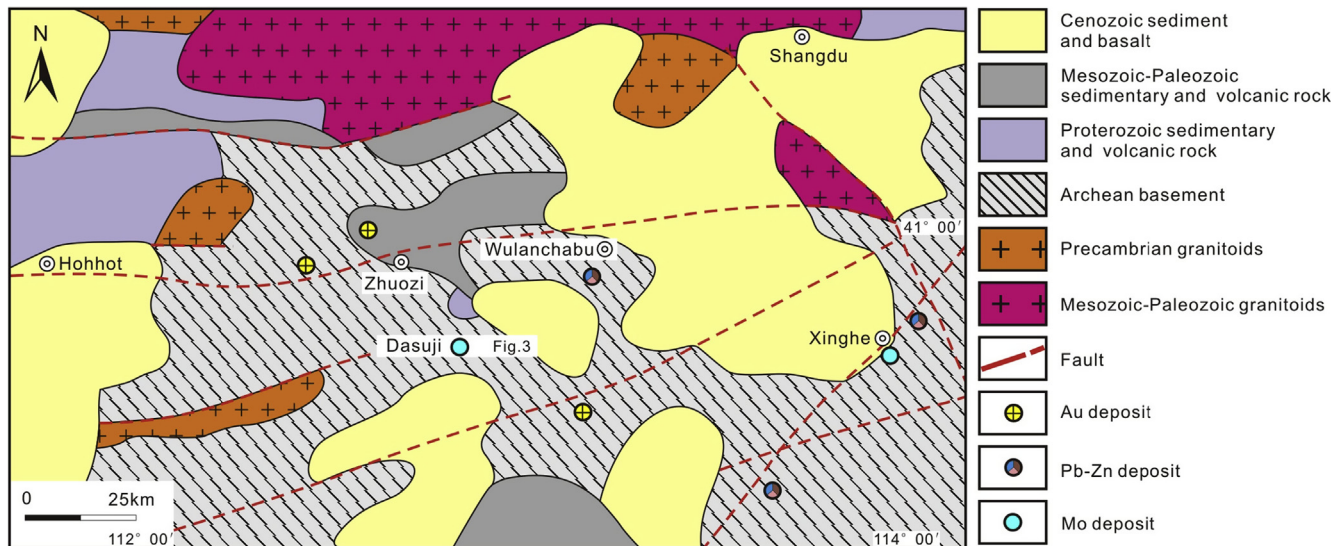


Fig. 2. Geological sketch map and distribution of the Mo deposits in central Inner Mongolia (after Wu, 2015).

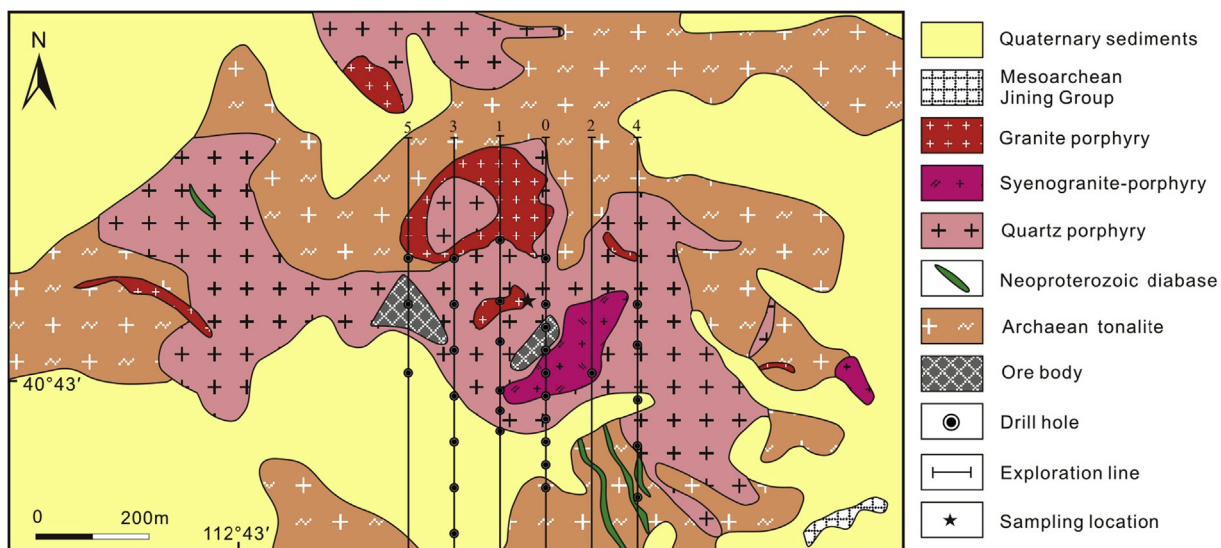


Fig. 3. Geological map of the Dasuji Mo deposit (after Wu, 2015).

Mesoarchean Jining Group and Quaternary sediments (Fig. 3). The Jining Group is composed of plagioclase gneiss and garnet-bearing leucogranulite. The intrusions include tonalite, quartz porphyry, syenogranite porphyry, and granite porphyry. The Mo mineralization occurs as disseminations, stockworks, and veinlets within the intrusive body, which occur as disseminations and stockworks in the granite porphyry (Fig. 4a, b) and as stockworks and veinlets in the quartz porphyry (Fig. 4c) and syenogranite porphyry. The granite porphyry is gray colored, porphyritic, and massive. The phenocrysts are mainly quartz, K-feldspar, and plagioclase and the matrix is composed of quartz, K-feldspar, and plagioclase, with minor accessory magnetite, zircon, and apatite. The content of the phenocryst in the rocks is approximately 25% and the content of the matrix is approximately 75%. Quartz mainly occurs as phenocrysts and groundmass, and the phenocrysts are characterized as subhedral and granular. The plagioclase phenocrysts are subhedral, tabular grains and have been altered to sericite. K-feldspar mainly occurs as phenocrysts and groundmass, and the phenocrysts are subhedral tabular and characterized by kaolinization. The orebodies in the Dasuji Mo deposit is asymmetrically lenticular (Fig. 5), strike nearly E-W with a length of 1100 m and a width of 360–450 m, and dip to the south at 40°–45° (Zhang et al., 2009a; Nie

et al., 2012; Wu, 2015). The dominant ore minerals in the Dasuji Mo deposits are molybdenite (Fig. 4d–e) and pyrite (Fig. 4f), with lesser amounts of magnetite, galena, and sphalerite. The gangue minerals are quartz, feldspar (Fig. 4g), sericite (Fig. 4h), and calcite (Fig. 4i), with minor fluorite, muscovite, and kaolinite. Hydrothermal alteration is well developed in the mining area, including silicification, K-feldspathization, sericitization, chloritization, epidotization, and carbonatization. Mineralization is spatially associated with silicification and sericitization and is not well-developed in the alteration zone (Nie et al., 2012). Mineralization has been divided into three paragenetic stages: (1) an early quartz–K-feldspar–pyrite–magnetite stage, (2) a middle quartz–molybdenite–pyrite stage, and (3) a late quartz–carbonate–pyrite–galena–sphalerite stage (Wu, 2015).

4. Samples and analytical methods

4.1. Samples

All representative samples of the granite porphyry were collected from an outcrop in the Dasuji Mo deposit. The whole-rock major and trace elements and the Sr–Nd isotopic compositions of four samples

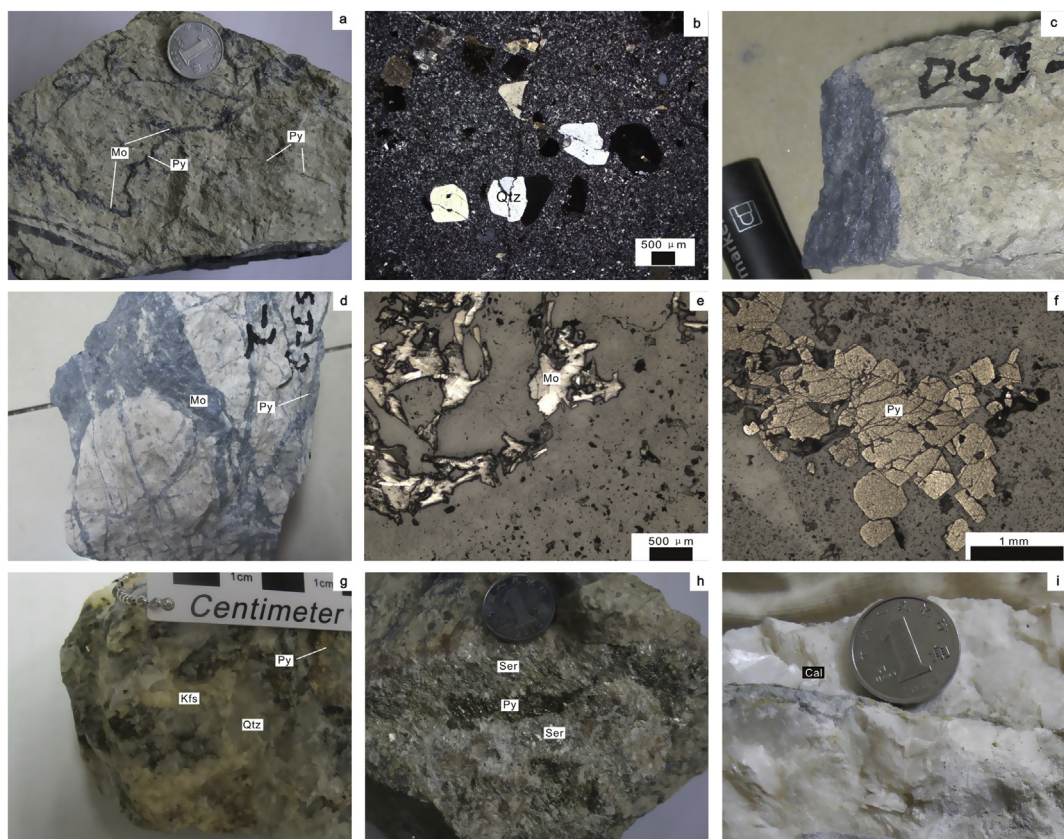


Fig. 4. Representative photographs of rock and ore samples from the Dasuji deposit. Qtz = quartz; Mo = molybdenite; Py = pyrite; Ser = sericite; Kfs = K-feldspar; Cal = calcite.

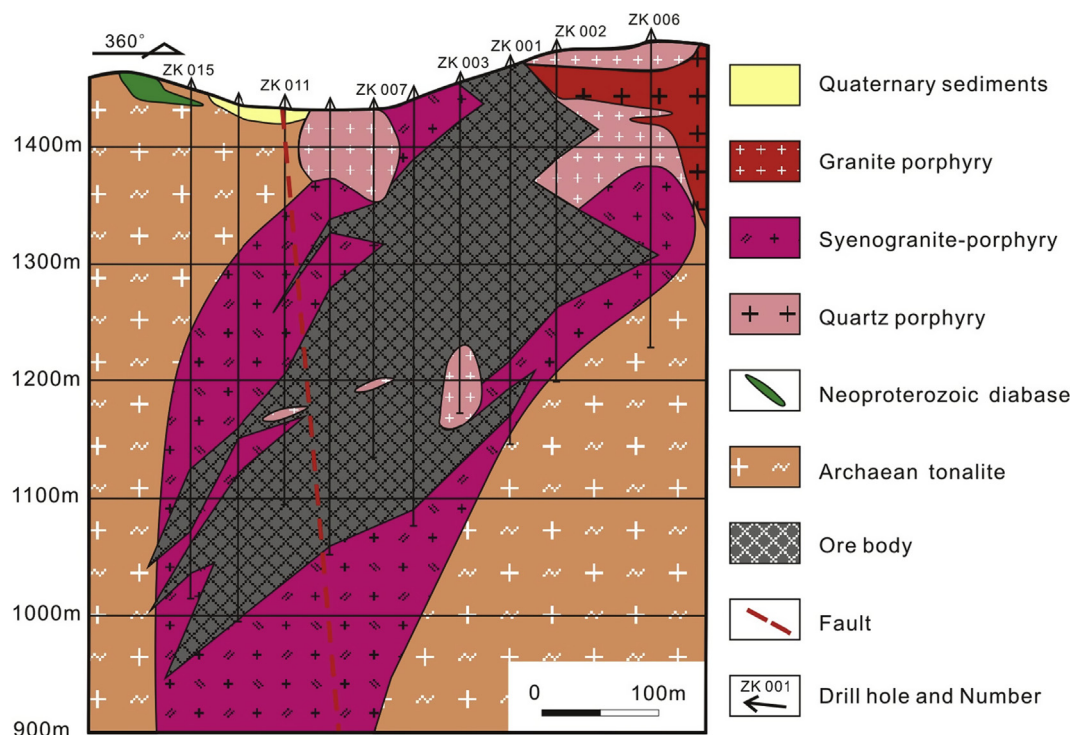


Fig. 5. Geological cross-section along the exploration line No. 0 of the Dasuji deposit (IMNMGEB, 2013).

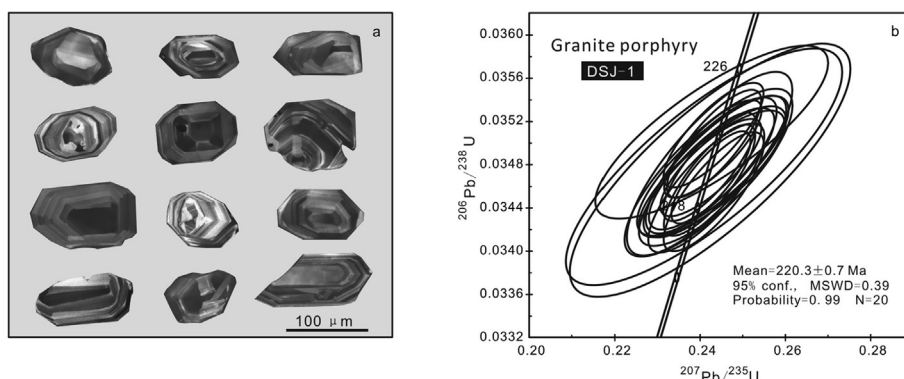


Fig. 6. Cathodoluminescence images of zircons (a) and U-Pb concordia diagram of zircons (b) of the granite porphyry.

were determined (DSJ-1a, DSJ-1b, DSJ-1c, DSJ-1d); one granite porphyry sample (DSJ-1a) was used for zircon U-Pb dating and Hf isotopic analysis. The Re-Os isotopic compositions of five molybdenite samples from thin mineralized granite porphyry (DSJ-3, DSJ-4 and DSJ-15) and quartz-molybdenite veins (DSJ-11 and DSJ-18) were determined.

4.2. Major and trace element determinations

Major and trace element analyses were carried out at the National Research Center for Geoanalysis, Beijing. The major elements were analyzed by X-ray fluorescence (XRF) spectrometry, with analytical uncertainties $\leq 5\%$. Ferric and ferrous iron measurements were determined by wet chemical analyses (titration). The analytical precision for the major oxides was based on certified standards (GSR-1 and GSR-3). Trace elements were determined by solution ICP-MS performed at the ICP-MS Laboratory of the National Research Center for Geoanalysis, Beijing. The detailed sample preparation, instrument operating conditions and calibration procedures followed Grégoire (2000).

4.3. LA-ICP-MS zircon U-Pb dating

Zircon grains were separated from the bulk samples using conventional techniques of density and magnetic separation. Representative zircon grains were handpicked under a binocular microscope, mounted in epoxy resin, polished, coated with gold, and mounted. Transmitted light and reflected-light images were taken under an optical microscope. The U-Pb isotopic analyses were performed using an Agilent 7700e mass spectrometer connected to a 193 nm ArF excimer laser ablation system at the Wuhan Sample Solution Analytical Technology Co., Ltd, Wuhan, China. Zircon 91,500 and glass NIST610 were used as external standards for U-Pb dating and trace element calibration, respectively. Both standard and unknown zircon analyses were measured with a 32 μm ablation spot size. Detailed operating conditions for the laser ablation system, the LA-ICP-MS instrument, and data reduction were described by Zong et al. (2017). Errors of individual analyses by LA-ICP-MS are quoted at the 1σ level, whereas errors on pooled ages are quoted at the 95% confidence level. The data were processed using the GLITTER and ISOPLOT (Ludwig, 2003) programs.

4.4. Molybdenite Re-Os dating

Molybdenite samples were collected from the Dasuji Mo deposit. Gravity and magnetic separation techniques were applied to crushed samples, and molybdenite grains were handpicked under a binocular microscope (purity > 99%). Re-Os isotope analyses were performed at the Re-Os Laboratory, National Research Center of Geoanalysis, Chinese Academy of Geological Sciences, Beijing, China. The chemical procedure followed Li et al. (2010). The model ages were calculated as

follows: $t = (\ln(1 + ^{187}\text{Os}/^{187}\text{Re}))/\lambda$, where λ is the decay constant of ^{187}Re , $1.666 \times 10^{-11}/\text{yr}^{-1}$ (Smolar et al., 1996).

4.5. Zircon Lu-Hf isotope analyses

In situ zircon Hf isotope analyses were performed using a NewWave UP193FX laser-ablation microprobe attached to a Neptune multi-collector ICP-MS at the State Key Laboratory for Mineral Deposits Research, Nanjing University, Nanjing. Hf isotope analysis was performed directly on top of the U-Pb laser ablation sites. The instrumental conditions and data acquisition were comprehensively described by Wu et al. (2006), Hou et al. (2007) and Geng et al. (2017). The $^{176}\text{Hf}/^{177}\text{Hf}$ ratios obtained for standard zircon MT is 0.282504 ± 14 (2σ) in this study. The present $^{176}\text{Hf}/^{177}\text{Hf}$ and $^{176}\text{Lu}/^{177}\text{Hf}$ ratios of chondrite and depleted mantle are 0.282772 and 0.0332, and 0.28325 and 0.0384, respectively (Blichert-Toft and Albarède, 1997; Griffin et al., 2000). $\lambda = 1.865 \times 10^{-11} \text{ year}^{-1}$ (Scherer et al., 2001). The Hf model ages were calculated as described in Nowell et al. (1998), Amelin et al. (2000) and Griffin et al. (2000).

4.6. Sr and Nd isotope analyses

The samples selected for Sr and Nd isotopic analyses were ground with an agate mill, and the powders were spiked with mixed isotope tracers, dissolved in Teflon capsules with HF + HNO₃ + HClO₄ acid, and separated by conventional cation-exchange techniques with diluted HBr as an eluent. The isotopic measurements were performed on a Finnigan MAT-262 mass spectrometer at the China National Nuclear Corporation Beijing Research Institute of Uranium Geology. The mass fractionation corrections for the Sr and Nd isotopic ratios were based on $^{86}\text{Sr}/^{88}\text{Sr} = 0.1194$ and $^{146}\text{Nd}/^{144}\text{Nd} = 0.7219$. Repeat analyses yielded a $^{87}\text{Sr}/^{86}\text{Sr}$ ratio of 0.710250 ± 7 for the NBS-987 Sr standard and a $^{143}\text{Nd}/^{144}\text{Nd}$ ratio of 0.512118 ± 3 for the JNd-1 Nd standard.

5. Results

5.1. Zircon LA-ICP-MS U-Pb geochronology

The separated zircons are euhedral or subhedral, colorless and transparent and show oscillatory zoning (Fig. 6a). The results of the zircon LA-ICP-MS U-Pb dating undertaken during this study are given in Table 1. The majority of these analyses are concordant or nearly concordant (Fig. 6b). The zircons from the granite porphyry sample DSJ-1 yielded $^{206}\text{Pb}/^{238}\text{U}$ ages from 218.4 to 222.4 Ma, with a weighted mean $^{206}\text{Pb}/^{238}\text{U}$ age of $220.3 \pm 0.7 \text{ Ma}$ ($n = 20$; mean squared weighted deviation (MSWD) = 0.39; Fig. 6b).

Table 1

Zircon U-Pb data from the Dasuji Mo deposit.

NO.	Th (ppm)	U (ppm)	Th/U	$^{207}\text{Pb}/^{206}\text{Pb}$	1 σ	$^{207}\text{Pb}/^{235}\text{U}$	1 σ	$^{206}\text{Pb}/^{238}\text{U}$	1 σ	$^{207}\text{Pb}/^{206}\text{Pb}$	1 σ	$^{207}\text{Pb}/^{235}\text{U}$	1 σ	$^{206}\text{Pb}/^{238}\text{U}$ (Ma)	1 σ
DSJ-1-1	298	179	1.7	0.050374	0.0030	0.243051	0.0145	0.034783	0.0005	213.0	132.4	220.9	11.9	220.4	3.3
DSJ-1-2	723	355	2.0	0.050551	0.0020	0.24308	0.0093	0.034941	0.0004	220.4	90.7	220.9	7.6	221.4	2.3
DSJ-1-3	282	233	1.2	0.051266	0.0037	0.242307	0.0159	0.034803	0.0007	253.8	168.5	220.3	13.0	220.5	4.3
DSJ-1-4	672	315	2.1	0.050915	0.0057	0.242478	0.0268	0.034743	0.0010	235.3	240.7	220.4	21.9	220.2	6.0
DSJ-1-5	339	286	1.2	0.050836	0.0020	0.242592	0.0097	0.034768	0.0004	231.6	92.6	220.5	7.9	220.3	2.3
DSJ-1-6	753	351	2.1	0.05101	0.0031	0.242976	0.0141	0.034689	0.0005	242.7	137.9	220.9	11.5	219.8	3.3
DSJ-1-7	481	248	1.9	0.050983	0.0026	0.242791	0.0120	0.034757	0.0005	239.0	114.8	220.7	9.8	220.2	2.9
DSJ-1-8	495	204	2.4	0.050588	0.0026	0.242687	0.0126	0.034787	0.0005	220.4	121.3	220.6	10.3	220.4	3.2
DSJ-1-9	253	175	1.4	0.050937	0.0057	0.241054	0.0264	0.034774	0.0009	239.0	237.0	219.3	21.6	220.4	5.6
DSJ-1-10	404	271	1.5	0.050247	0.0018	0.243349	0.0090	0.034987	0.0004	205.6	83.3	221.2	7.4	221.7	2.5
DSJ-1-11	169	126	1.3	0.051765	0.0037	0.242058	0.0161	0.034721	0.0006	276.0	164.8	220.1	13.2	220.0	3.9
DSJ-1-12	426	285	1.5	0.050247	0.0018	0.242332	0.0089	0.034774	0.0004	205.6	83.3	220.3	7.3	220.4	2.6
DSJ-1-13	162	81	2.0	0.050203	0.0045	0.242859	0.0223	0.035094	0.0007	211.2	255.5	220.8	18.2	222.4	4.1
DSJ-1-14	366	264	1.4	0.050619	0.0018	0.242297	0.0088	0.034651	0.0004	233.4	83.3	220.3	7.2	219.6	2.6
DSJ-1-15	259	196	1.3	0.050318	0.0028	0.242789	0.0140	0.034709	0.0005	209.3	136.1	220.7	11.4	220.0	3.0
DSJ-1-16	418	303	1.4	0.051249	0.0199	0.243223	0.0096	0.035068	0.0004	222.3	223.7	222.8	24.6	222.2	4.7
DSJ-1-17	155	112	1.4	0.051073	0.0030	0.243549	0.0137	0.034777	0.0005	242.7	135.2	221.3	11.2	220.4	3.3
DSJ-1-18	236	326	0.7	0.051019	0.0020	0.243278	0.0096	0.034545	0.0004	242.7	90.7	218.6	7.9	218.4	2.8
DSJ-1-19	255	433	0.6	0.050709	0.0016	0.24263	0.0076	0.034677	0.0003	227.8	75.9	218.1	6.2	219.3	2.2
DSJ-1-20	157	256	0.6	0.050545	0.0023	0.241538	0.0111	0.034579	0.0005	220.4	99.1	219.7	9.1	219.1	3.0

Table 2

Results of Re-Os isotopic analyses of molybdenite from the Dasuji Mo deposit.

Sample no.	Re ($\mu\text{g.g}^{-1}$)	^{187}Re ($\mu\text{g.g}^{-1}$)	^{187}Os (ng.g^{-1})	Model age (Ma)				
DSJ-3	9.23	0.07	5.802	0.046	21.05	0.16	217.4	3.2
DSJ-4	17.56	0.16	11.039	0.099	40.51	0.29	219.8	3.3
DSJ-11	10.00	0.16	6.286	0.100	23.01	0.16	219.3	4.4
DSJ-15	9.86	0.07	6.200	0.046	22.62	0.26	218.6	3.7
DSJ-18	17.97	0.22	11.294	0.140	41.45	0.36	219.9	4.0

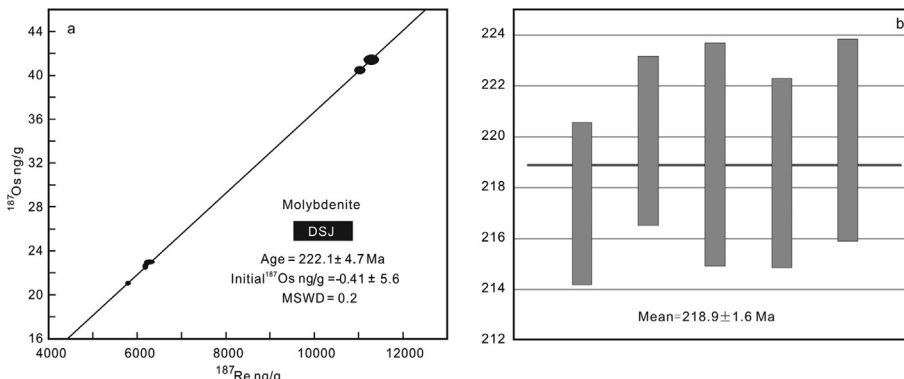


Fig. 7. Re-Os isotopic isochron (a) and the weighted mean ages (b) for the molybdenite separated from the Dasuji Mo deposit.

5.2. Molybdenite Re-Os geochronology

The Re-Os isotopic data during this study are given in Table 2, with the molybdenite Re-Os isochron and weighted mean model age shown in Fig. 7. These five molybdenite samples yielded model ages of 217.4–219.9 Ma, with a well-defined $^{187}\text{Re}-^{187}\text{Os}$ isochron age of 222.1 ± 4.7 Ma (MSWD = 0.20; Fig. 7a) and a weighted mean model age of 218.9 ± 1.6 Ma (Fig. 7b). These samples have initial ^{187}Os concentrations of -0.41 ± 0.56 ppb, and the nearly identical ages yielded by both isochron and model approaches indicate that these results are reliable.

5.3. Major and trace element geochemistry

The whole-rock major and trace element compositions of the granite porphyry are listed in Table 3. All of the analyzed samples are classified as subalkaline series (Fig. 8a; Irvine and Baragar, 1971) peraluminous

rocks (Fig. 8b; Maniar and Piccoli, 1989). The granite porphyry contains 76.15–77.97 wt% SiO_2 , 12.11–12.40 wt% Al_2O_3 , 0.11–0.37 wt% CaO , 2.32–2.78 wt% Na_2O , 4.71–5.03 wt% K_2O , and 7.35–7.49 wt% $\text{Na}_2\text{O} + \text{K}_2\text{O}$. Plotting the data for these samples in a K_2O vs. SiO_2 diagram indicates that they are high-K calc-alkaline series rocks (Fig. 8c; Peccerillo and Taylor, 1976).

The chondrite-normalized rare earth element (REE) compositions of the samples analyzed during this study are shown in Fig. 9a. All of these samples are enriched in the light REEs (LREEs) and are depleted in the heavy REEs (HREEs), with total REE concentrations of 87.89–103.83 ppm and strong negative Eu anomalies ($\delta\text{Eu} = 0.21$ –0.28). Plotting the data for these granite porphyry samples on a primitive-mantle-normalized multielement variation diagram indicates that they are all enriched in Rb, Th, U, Zr, and Hf and depleted in Ba, P, and Ti (Fig. 9b).

Table 3

Major (wt%) and trace elements (ppm) data of the granite porphyry.

Sample	DSJ-1a	DSJ-1b	DSJ-1c	DSJ-1d	Sample	DSJ-1a	DSJ-1b	DSJ-1c	DSJ-1d
SiO ₂	77.97	76.15	77.35	77.95	Ga	24	23	22.9	24.6
Al ₂ O ₃	12.21	12.4	12.39	12.11	Y	18.6	32.5	30.8	18.4
TiO ₂	0.08	0.08	0.07	0.08	La	23.2	24.3	26.2	24
TE ₂ O ₃	0.96	1.71	1.18	1.14	Ce	36.8	41.2	43.8	40.1
CaO	0.11	0.37	0.25	0.13	Pr	4.01	4.25	4.55	4.11
MgO	0.12	0.16	0.13	0.13	Nd	11.1	12	12.5	11.5
K ₂ O	4.94	4.71	4.97	5.03	Sm	1.86	2.16	2.12	1.87
Na ₂ O	2.52	2.78	2.48	2.32	Eu	0.12	0.17	0.19	0.13
MnO	0.06	0.13	0.05	0.06	Gd	1.62	1.99	2.04	1.64
P ₂ O ₅	0.01	0.01	0.01	0.01	Tb	0.34	0.43	0.43	0.33
LOI	2.58	3.39	2.82	2.47	Dy	2.2	3.07	3.06	2.2
Mg#	0.71	0.65	0.69	0.70	Ho	0.55	0.79	0.77	0.54
Ba	139	384	156	139	Er	1.91	2.76	2.69	1.95
Hf	6.32	5.95	5.8	6.3	Tm	0.38	0.53	0.51	0.36
Ta	8.24	7.62	8	8.27	Yb	3.25	4.39	4.27	3.28
Pb	73.4	60.7	41.1	98.5	Lu	0.55	0.73	0.7	0.54
Th	52.3	53.7	56	52	ΣREE	87.89	98.77	103.83	92.55
U	9.05	10.2	9.53	9.48	LREE	77.09	84.08	89.36	81.71
Rb	379	367	392	397	HREE	10.80	14.69	14.47	10.84
Sr	66.2	42.1	57.8	65.3	LREE/HREE	7.14	5.72	6.18	7.54
Zr	98.3	96.3	100	103	La _N /Yb _N	5.12	3.97	4.40	5.25
Nb	131	144	150	131	δEu	0.21	0.25	0.28	0.22

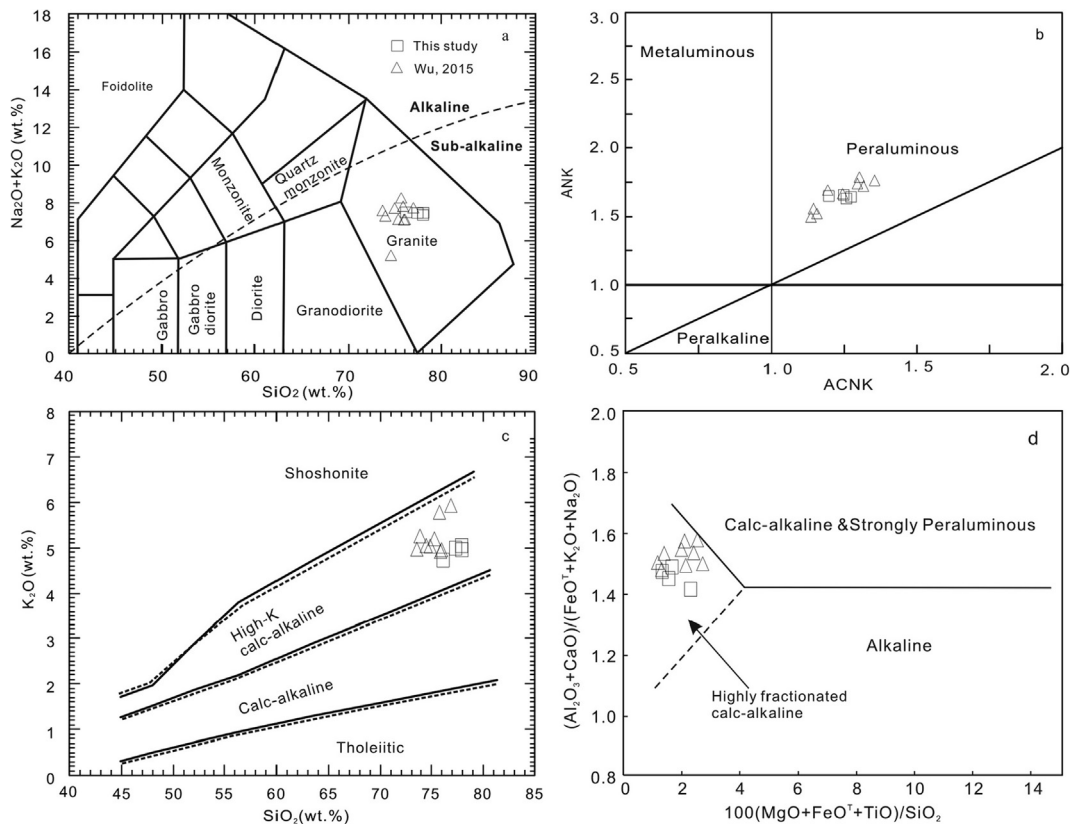


Fig. 8. (a) SiO_2 versus $(\text{Na}_2\text{O} + \text{K}_2\text{O})$ plot (Middlemost, 1994), (b) A/NK ($\text{Al}_2\text{O}_3/(\text{Na}_2\text{O} + \text{K}_2\text{O})$) vs. A/CNK ($\text{Al}_2\text{O}_3/(\text{CaO} + \text{Na}_2\text{O} + \text{K}_2\text{O})$) diagram (Maniar and Piccoli, 1989), (c) SiO_2 versus K_2O plot of granites (Peccerillo and Taylor, 1976), (d) Major element discrimination of granites (Sylvester 1989).

5.4. Sr–Nd isotope composition

The Sr–Nd isotope compositions of the analyzed samples are shown in Table 4. The initial isotopic ratios of the granite porphyry are calculated based on the zircon U–Pb ages. The granite porphyry has initial $^{87}\text{Sr}/^{86}\text{Sr}$ ratios of 0.70516–0.70784, $\epsilon\text{Nd(t)}$ values from −13.9 to −12.8 (Fig. 10a), and Paleoproterozoic whole-rock ϵNd model ages of 2125–2033 Ma, with an average age of 2100 Ma.

5.5. Zircon Lu–Hf isotope data

The Lu–Hf isotopic compositions of a total of 10 zircons from sample DSJ-1 were determined during this study (Table 5) and yielded $^{176}\text{Hf}/^{177}\text{Hf}$ ratios and $\epsilon\text{Hf(t)}$ values of 0.282175–0.282236 and −16.4 to −7.3, respectively. These zircons yielded two-stage model ages (T_{DM2}) of 2293–17616 Ma, with an average age of 2149 Ma (Fig. 10b).

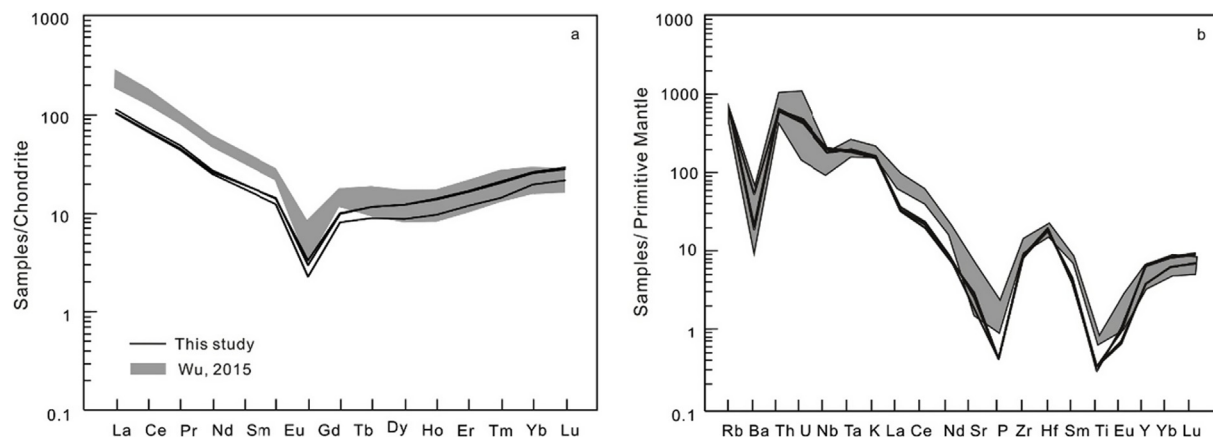


Fig. 9. Chondrite-normalized REE patterns (a, normalized values are from Boynton, 1984) and primitive mantle-normalized trace element patterns (b, normalized values are from Sun and McDonough, 1989) of the granite porphyry.

Table 4

Sr-Nd isotopic compositions of the granite porphyry.

Sample	Rb (ppm)	Sr (ppm)	$^{87}\text{Rb}/^{86}\text{Sr}$	$^{87}\text{Sr}/^{86}\text{Sr}$	$(^{87}\text{Sr}/^{86}\text{Sr})_i$	Sm	Nd	$^{147}\text{Sm}/^{144}\text{Nd}$	$^{143}\text{Nd}/^{144}\text{Nd}$	$(^{143}\text{Nd}/^{144}\text{Nd})_i$	$\epsilon_{\text{Nd}}(t)$	T _{DM2}
DSJ-1a	379	66.2	16.566	0.7592	0.70733	1.86	11.1	0.1013	0.5118	0.511644	-13.9	2124
DSJ-1b	367	42.1	25.225	0.7857	0.70682	2.16	12	0.1088	0.5119	0.511701	-12.8	2033
DSJ-1c	392	57.8	19.624	0.7666	0.70516	2.12	12.5	0.1026	0.5118	0.511647	-13.8	2119
DSJ-1d	397	65.3	17.592	0.7629	0.70784	1.87	11.5	0.0983	0.5118	0.511643	-13.9	2125

Notes: ^{87}Rb decay $\lambda = 1.42 \times 10^{-11} \text{ year}^{-1}$; ^{147}Sm decay $\lambda = 6.54 \times 10^{-12} \text{ year}^{-1}$; The $^{143}\text{Nd}/^{144}\text{Nd}$ and $^{147}\text{Sm}/^{144}\text{Nd}$ ratios of chondrite and depleted mantle at present day are 0.512638 and 0.1967, 0.51315 and 0.2137, respectively (Jacobsen and Wasserburg, 1980).

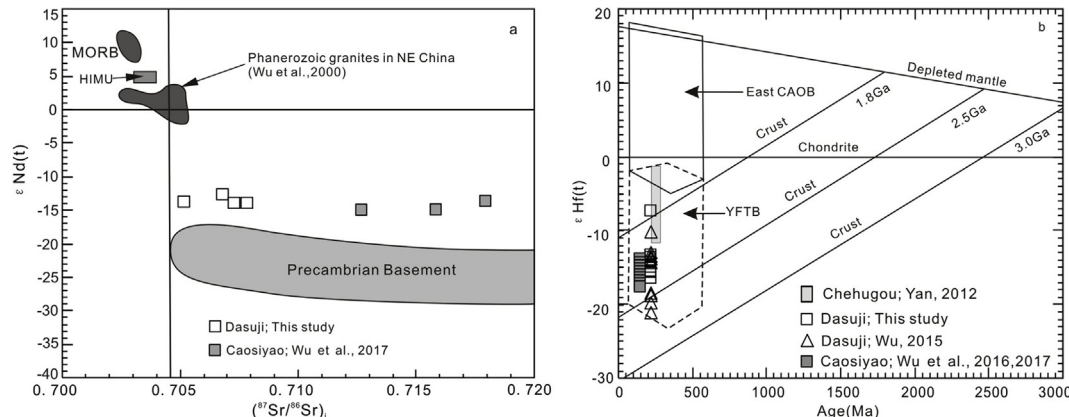


Fig. 10. Variations in $(^{87}\text{Sr}/^{86}\text{Sr})_i$ versus $\epsilon_{\text{Nd}}(t)$ (a, Jahn et al., 1999) and $\epsilon_{\text{Hf}}(t)$ versus the crystallization age of the zircons (b, Yang et al., 2006) for the Dasuji granite porphyry. The Hf isotopic evolution line of the Archean average crust with $^{176}\text{Lu}/^{177}\text{Hf} = 0.015$ is after Griffin et al. (2000). The fields for the East Xing-Meng (Xing'an–Mongolian Orogenic Belt) and Yanshan igneous rocks are from Yang et al. (2006).

Table 5

Zircon Hf isotopic compositions of the granite porphyry.

Spot no.	Age (Ma)	$^{176}\text{Yb}/^{177}\text{Hf}$	$^{176}\text{Lu}/^{177}\text{Hf}$	$^{176}\text{Hf}/^{177}\text{Hf}$	2σ	$\epsilon_{\text{Hf}}(0)$	$\epsilon_{\text{Hf}}(t)$	T _{DM1} (Ma)	T _{DM2} (Ma)	f _{Lu/Hf}
1	220.4	0.022777	0.000811	0.282200	0.000020	-20.2	-15.5	1475	2236	-0.98
2	221.4	0.028979	0.000993	0.282255	0.000022	-18.3	-13.6	1406	2116	-0.97
3	220.5	0.098732	0.003419	0.282229	0.000030	-19.2	-14.9	1541	2195	-0.90
4	220.2	0.039701	0.001427	0.282267	0.000021	-17.8	-13.2	1405	2092	-0.96
5	220.3	0.036011	0.001479	0.282436	0.000017	-11.9	-7.3	1168	1716	-0.96
6	219.8	0.029090	0.001099	0.282235	0.000024	-19.0	-14.3	1438	2162	-0.97
7	220.2	0.110618	0.003657	0.282208	0.000021	-19.9	-15.6	1583	2243	-0.89
8	220.4	0.039606	0.001369	0.282202	0.000020	-20.2	-15.5	1495	2237	-0.96
9	220.4	0.025398	0.000902	0.282175	0.000021	-21.1	-16.4	1514	2293	-0.97
10	221.7	0.040966	0.001383	0.282217	0.000021	-19.6	-15.0	1474	2202	-0.96

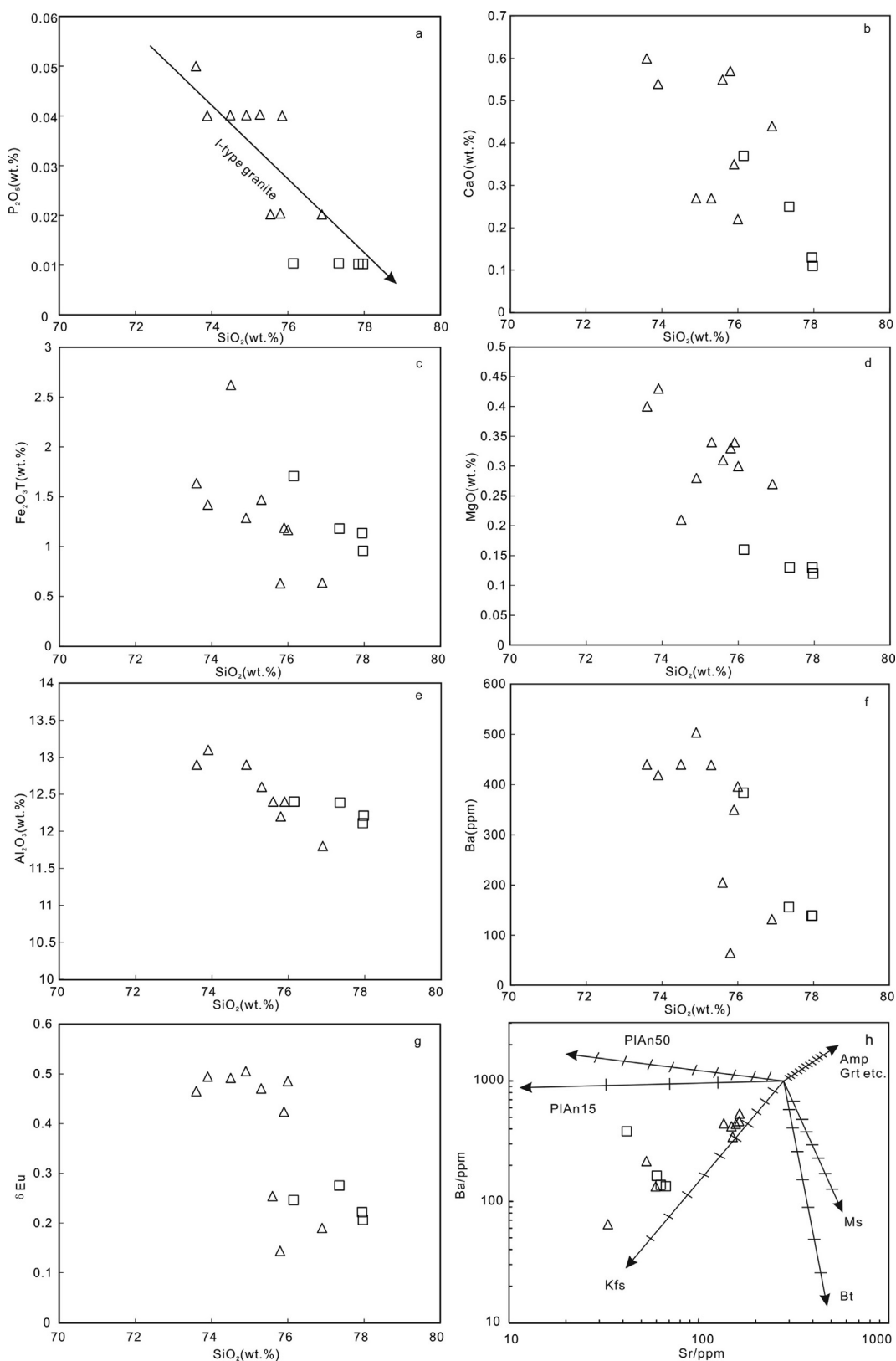


Fig. 11. (a–g) Selected oxide and trace element plots for the granite porphyry in the Dasuji Mo deposit. (h) Sr versus Ba plots for the granite porphyry (Li et al., 2017a). The symbols are the same as in Fig. 8. PlAn50, plagioclase ($An = 50$); PlAn15, plagioclase ($An = 15$); Kfs, K-feldspar; Amp, amphibole; Grt, garnet; Ms, muscovite; Bt, biotite.

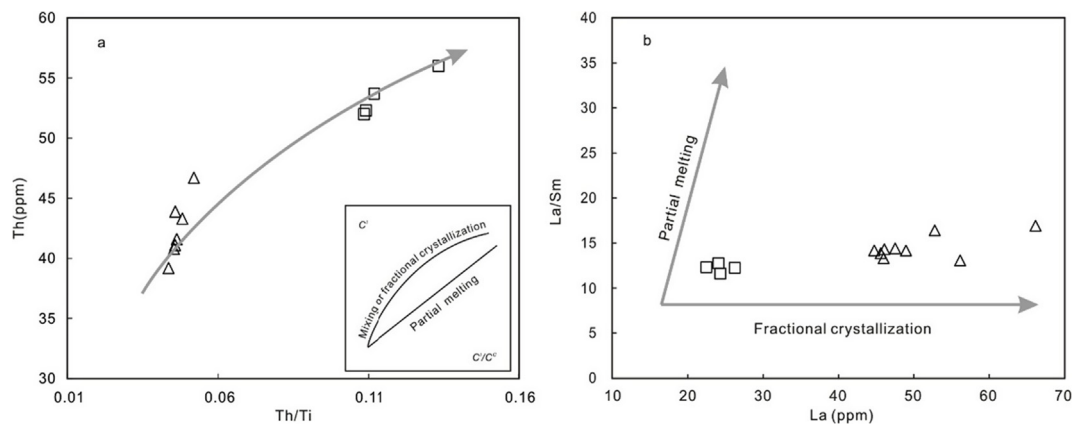


Fig. 12. Petrogenetic diagrams for the granite porphyry. (a) Th vs. Th/Ti diagram (Schiano et al., 2010). (b) La/Sm vs. La diagram (Cocherine, 1986). The inset is a schematic C^l versus C^l/C^c diagram (C^l , incompatible element concentration, and C^c , compatible element concentrations). The symbols are the same as in Fig. 8.

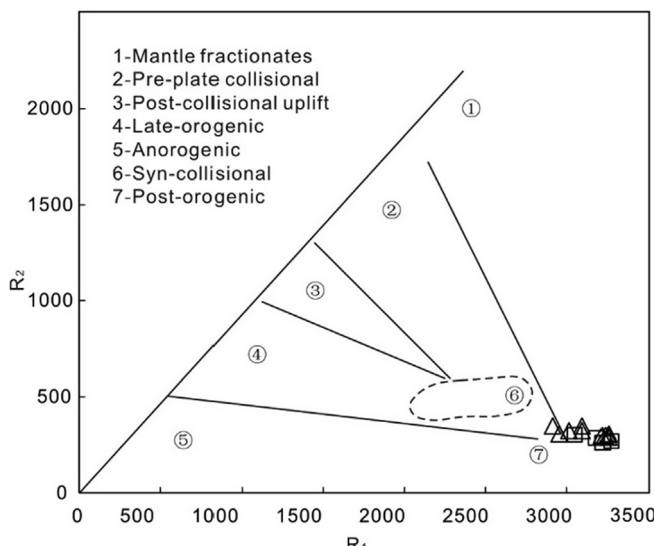


Fig. 13. R₁–R₂ tectonic discrimination diagram of the granite porphyry (Batchelor and Bowden, 1985). R₁ = 4Si-11(Na + K) - 2(Fe + Ti); R₂ = 6Ca + 2Mg + Al. The symbols are the same as in Fig. 8.

6. Discussion

6.1. Magmatism and mineralization timing

Numerous Mo deposits have been discovered in the northern margin

of the NCB, for which isotopic age data have been published, and the timing of formation of the Mo deposits in the study area occurred in three main stages: late Permian-Triassic, Jurassic, and Cretaceous Mo metallogeny that generated abundant Jurassic and the Cretaceous Mo deposits (Zhang et al., 2010a; Liu et al., 2010; Zeng et al., 2011, 2012a, 2012b, 2012c, 2013; Chen et al., 2012, 2016; Sun et al., 2012; Shu et al., 2014; 2015, 2016; Zhao, 2016; Wu et al., 2008, 2017). The ages for the Dasuji Mo deposit have been reported in a number of other studies, including Yu et al. (2008) and Li (2012), who suggested that the Mo mineralization occurred during the Yanshanian based on intrusions in the deposit. Zhang et al. (2009a) reported a molybdenite Re-Os isochron age of 222.5 ± 3.2 Ma, which suggests that the deposit formed during the Late Triassic. Wu (2015) obtained LA-ICP-MS U-Pb ages of 234 ± 3 Ma, 230 ± 5 Ma, and 224 ± 4 Ma for the quartz porphyry, syenogranite porphyry, and granite porphyry, respectively, and a molybdenite Re-Os isochron age of 223.5 ± 5.5 Ma, which suggests that the deposit formed in the Late Triassic. Our new zircon U-Pb data suggest that the crystallization age of the granite porphyry is 220.3 ± 0.7 Ma, and the molybdenite Re-Os isochron age is 218.9 ± 1.6 Ma, which suggests that the Dasuji Mo mineralization and magmatism occurred during the Late Triassic rather than the Yanshanian (Yu et al., 2008; Li, 2012), which is consistent with the timing of magmatism in the northern margin of the NCB (Zhang et al., 2010b). Therefore, combining the existing dates with our new U-Pb and Re-Os ages indicates that mineralization and magmatism were contemporaneous during the formation of the Dasuji porphyry Mo deposit and that Mo mineralization occurred during the Late Triassic.

Numerous Mo deposits have been discovered in northeast China, for which isotopic age data have been reported by other workers

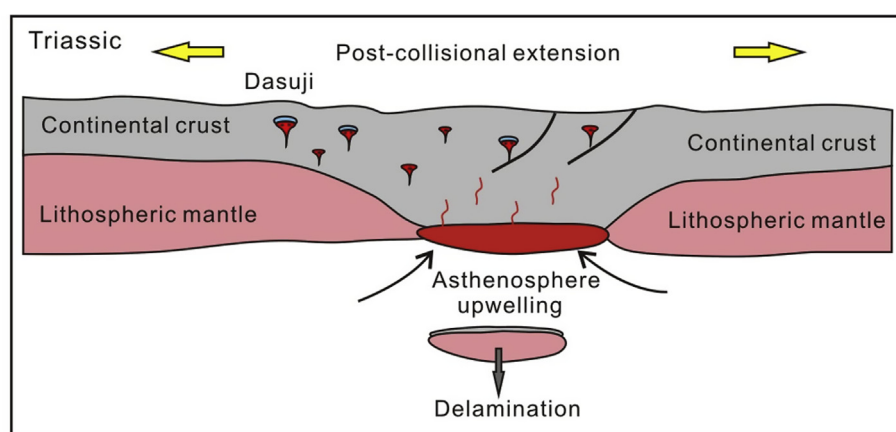


Fig. 14. Genetic model for the Dasuji Mo deposit (after Shu et al., 2016; Gao et al., 2017).

(Supplement Table 1). The Mo deposits in this region formed between 476 and 111 Ma during the Ordovician (~476 Ma), Triassic (250–203 Ma), Jurassic (200–140 Ma), and Cretaceous (139–111 Ma) periods. Large-scale Mo mineralization occurred during the Jurassic but numerous Triassic Mo deposits have been discovered in the NCB in recent years, which indicate that the Triassic Mo mineralization has a huge exploration potential in this region.

6.2. Petrogenesis of the ore-bearing granite porphyry

Correctly identifying the genetic types of magmatic rocks is significant for understanding the magma source regions and tectonic settings (Pearce et al., 1984; Sylvester, 1989; Barbarin, 1999; Yang et al., 2015a). Fractionated I-type granites are difficult to distinguish from A-type granites, and the extremely felsic A-type granites ($\text{SiO}_2 > 72\%$) have the same chemical and mineralogical characteristics as felsic, fractionated I-type granites (King et al., 1997). However, some different characteristics of A-type granites and fractionated I-type granites have been previously identified (Whalen et al., 1987; King et al., 1997; Wang et al., 2000; Yang et al., 2015b). The granite porphyry is highly siliceous (up to 76.2%), and amphibole and muscovite are absent. The data obtained in this study indicate that the granites samples are alkali rich and have high SiO_2 , and the differentiation index ranges from 93 to 95; the samples are plotted in the highly fractionated calc-alkaline granites field (Fig. 8d). Negative correlations are presented between P_2O_5 and SiO_2 (Fig. 11a). Moreover, the calculated zircon saturation temperatures (T_{zr}) of the granite porphyry are 762–774 °C (average 768 °C); the calculation values are comparatively inconsistent with the fractionated I-type granite (764 °C, King et al., 1997; Qiu and Deng, 2017). Therefore, we suggest that the Mo mineralization-related granites are the highly fractionated I-type.

The granite porphyry is characterized by negative $\varepsilon\text{Nd(t)}$ values and old Nd two-stage model ages, which is different from the Phanerozoic granites in NE China (Wu et al., 2000; Fig. 10a). The zircon $\varepsilon\text{Hf(t)}$ values are also similar; the rocks show negative $\varepsilon\text{Hf(t)}$ values, and in the $\varepsilon\text{Hf(t)}$ vs. age diagram (Fig. 10b), the samples plot in the Yanshan Fold and Thrust Belt (YFTB) field (Yang et al., 2006). All these data points show a spread of $\varepsilon\text{Hf(t)}$ values that plot near but slightly higher than the ~2.5 Ga evolution line of the lower crust of the NCB, which indicates that the magma sources were mainly derived from the ancient lower crust, although mantle material melts into the lower crust cannot be ruled out. The Sr-Nd-Hf data indicate that the granite porphyry was derived from the partial melting of ancient lower crust, which is consistent with the Mo deposits in the northern margin of the NCB (Fig. 10), and thus suggests that they have similar magma sources (Wu et al., 2016; Qiu et al., 2017). Therefore, we suggest that the parental magma of the Dasuji granite porphyry predominantly originated from ancient lower crust materials.

The Dasuji granite porphyry displays linear correlations between SiO_2 and other major and trace element concentrations (Castillo et al., 1999; Qiu et al., 2018; Fig. 11a–g), which indicates that these magmas most likely fractionate minerals such as plagioclase, potassium feldspar, hornblende, and various accessory minerals during magma evolution. All of these samples have strongly negative Eu anomalies ($\delta\text{Eu} = 0.21\text{--}0.28$), which indicates the fractional crystallization of feldspar (Fig. 11h). Moreover, the data for these samples define a curving array on the Th/Ti vs. Th diagram (Schiano et al., 2010; Fig. 12a), and the La/Sm vs. La diagram shows that the granite porphyry samples are distributed along the fractional crystallization line (Fig. 12b), which suggests that the dominant control on their compositions was fractional crystallization.

6.3. Geodynamic setting

The northern margin of the NCB is located between the NCB and the Central Asian Orogenic Belt (CAOB); this area was significantly affected

by the evolution and final closure of the Paleo-Asian Ocean. However, the timing of the final closure of the Paleo-Asian ocean is still controversial, with a suggested timing of the Late Devonian to early Carboniferous (Tang, 1990; Xu et al., 2013; Zhao et al., 2013; Zhao and Zhai, 2013), the middle Permian (Li et al., 2014) and the middle Paleozoic to Early Triassic (Xiao et al., 2003; Li et al., 2006; Zhang et al., 2009d; Wilde, 2015). However, based on regional chronology and petrology information, the Later Triassic magmatic belt was formed in NE China and is represented by the ultramafic-syenitic complex, the alkaline complex, A-type granites and A-type rhyolites (Han et al., 2004; Wu et al., 2004; Xu et al., 2009; Zhang et al., 2009e; Zhu et al., 2016; Niu et al., 2012, 2017), which defines the closure of the Paleo-Asian Ocean followed by post-collisional extension (Shao et al., 2000; Zhao et al., 2010; Zhang et al., 2009e, 2010b; Chen et al., 2013; Qiu et al., 2014). In addition, molasse sequences have been identified to the east of the NCB, which indicates that final closure of the Paleo-Asian Ocean took place before the Late Triassic (Li et al., 2017b; Xin et al., 2011; Wang et al., 2016b). In this study, the U-Pb and Re-Os ages indicate that granite porphyry (220 Ma) and molybdenite (219 Ma) in the Dasuji Mo deposit formed in the Late Triassic. We plotted the geochemical data in an R1–R2 diagram (Fig. 13; Batchelor, 1985). Fig. 13 shows that the Dasuji granite porphyry samples plot in the post-orogenic granite field. These data suggest that the mineralization-related granite porphyry was emplaced in a post-collisional setting, which is consistent with the tectonic setting of the mineralization-related granites associated with the Mo deposits of the NCB district (Zhang et al., 2010a; Zeng et al., 2012c; Duan et al., 2015; Shu et al., 2016; Gao et al., 2017). Therefore, during the Late Triassic and under post-collisional extension conditions, underplating magma not only triggered the partial melting of lower crust but also injected mantle melts into the lower crust melts, which resulted in magmatism and Mo mineralization. As mentioned above, the Late Triassic hydrothermal activity and mineralization in this region was triggered by the post-collisional extensional regime (Fig. 14).

7. Conclusions

Based on the zircon U-Pb, molybdenite Re-Os, geochemical, Sr-Nd isotope and zircon Hf isotope analyses of the granite porphyry of the Dasuji Mo deposit, we summarize our conclusions as follows:

- (1) Zircon grains from the granite porphyry yield a $^{206}\text{Pb}/^{238}\text{U}$ mean age of 220.3 Ma, which is similar to the molybdenite Re-Os weighted mean model age of 218.9 ± 1.6 Ma. These data indicate that magmatism and mineralization occurred during the late Triassic.
- (2) The granite porphyry is compositionally characterized by high SiO_2 and $\text{Na}_2\text{O} + \text{K}_2\text{O}$ contents, depletion of Ba, Sr, P and Ti, and enrichment in Rb, Th, U, Zr, and Hf. $\varepsilon\text{Nd(t)}$ and $\varepsilon\text{Hf(t)}$ values are strongly negative, which indicates that the magma was generated by the partial melting of ancient lower crust materials.
- (3) The Late Triassic magmatism and mineralization within the Dasuji Mo deposit formed in a post-collisional extensional setting.

Acknowledgments

This work was jointly supported by the National Key Research and Development Program of China (2017YFC0601303), the National Natural Science Foundation of China (No. 41602075), the Chinese Geological Survey Program (DD20160100), and the Basic Research of the Ministry of Science and Technology, China (No. 2014FY121000). In particular, we express our gratitude to Associate Editor Dr. Kunkeng Qiu and an anonymous reviewer for their critical reviews and excellent suggestions that improved this article.

Appendix A. Supplementary data

Supplementary data to this article can be found online at <https://doi.org/10.1016/j.oregeorev.2018.10.018>.

References

- Amelin, Y., Lee, D.C., Halliday, A.N., 2000. Early–middle Archaean crustal evolution deduced from Lu-Hf and U-Pb isotopic studies of single zircon grains. *Geochim. Cosmochim. Acta* 64, 4205–4225.
- Barbarin, B., 1999. A review of the relationships between granitoid types, their origins and their geodynamic environments. *Lithos* 605–626.
- Batchelor, R.A., Bowden, P., 1985. Petrogenetic interpretation of granitoid rock series using multicationic parameters. *Chem. Geol.* 48, 43–55.
- Blichert-Toft, J., Albarède, F., 1997. The Lu-Hf geochemistry of chondrites and the evolution of the mantle–crust system. *Earth Planet. Sci. Lett.* 148, 243–258 (Erratum: Earth Planet. Science Letters 154, 349).
- Boynton, W.V., 1984. Geochemistry of the rare earth elements: meteorite studies. In: Henderson, P. (Ed.), *Rare earth element geochemistry*. Elsevier, New York, pp. 63–114.
- Castillo, P.R., Janney, P.E., Solidum, R.U., 1999. Petrology and geochemistry of Camiguin island, southern Philippines: insights to the source of adakites and other lavas in a complex arc setting. *Contrib. Mineral. Petrol.* 134, 33–51.
- Chen, B., Niu, X.L., Wang, Z.Q., Gao, L., Wang, C., 2013. Geochronology, petrology, and geochemistry of the Yaojiazhuan ultramafic-syenitic complex from the North China Craton. *Sci. China: Earth Sci.* 56, 1294–1307.
- Chen, Y.J., Zhang, C., Li, N., Yang, Y.F., Deng, K., 2012. Geology of the Mo deposits in North-East China. *J. Jilin Univ. (Earth Sci. Ed.)* 42, 1223–1268 (in Chinese with English abstract).
- Chen, Y.J., Zhang, C., Wang, P., Pirajno, F., Li, N., 2016. The Mo deposits of Northeast China: a powerful indicator of tectonic settings and associated evolutionary trends. *Ore Geol. Rev.* 81, 602–640.
- Cocherine, A., 1986. Systematic use of trace element distribution patterns in log-log diagram for plutonic suites: *Geochim. Geochim. Cosmochim. Acta* 1, 2517–2522.
- Duan, X.X., Zeng, Q.D., Yang, Y.H., Liu, J.M., Chu, S.X., Sun, Y., Zhang, Z.L., 2015. Triassic magmatism and Mo mineralization in Northeast China: geochronological and isotopic constraints from the Laojiagou porphyry Mo deposit. *Int. Geol. Rev.* 57, 55–75.
- Gao, J., Klemd, R., Zhu, M.T., Wang, X.S., Li, J.L., Wan, B., Xiao, W.J., Zeng, Q.D., Shen, P., Sun, J.G., Qin, K.Z., Campos, E., 2017. Large-scale porphyry-type mineralization in the Central Asian metallogenic domain: a review. *J. Asian Earth Sci.* <https://doi.org/10.1016/j.jseas.2017.10.002>.
- Geng, J.Z., Qiu, K.F., Gou, Z.Y., Yu, H.C., 2017. Tectonic regime switchover of Triassic Western Qinling Orogen: Constraints from LA-ICP-MS zircon U-Pb geochronology and Lu-Hf isotope of Dangchuan intrusive complex in Gansu, China. *Chemie der Erde/Geochemistry* 77 (4), 673–674.
- Gregoire, M., Moine, B.N., O'Reilly, S.Y., Cottin, J.Y., Giret, A., 2000. Trace element residence and partitioning in mantle xenoliths metasomatized by highly alkaline, silicate-and carbonate-rich melts (Kerguelan Islands, Indian Ocean). *J. Petrol.* 41, 477–509.
- Griffith, W.L., Pearson, N.J., Belousova, E., Jackson, S.E., Van Achterbergh, E.O., Reilly, S.Y., Shee, S.R., 2000. The Hf isotope composition of cratonic mantle, LAM-MC-ICPMs analysis of zircon megacrysts in kimberlites. *Geochim. Cosmochim. Acta* 64, 133–147.
- Han, B.F., Kagami, H., Li, H., 2004. Age and Nd-Sr isotopic geochemistry of the Guangtoushan alkaline granite, Hebei province, China: implications for early Mesozoic crust–mantle interaction in North China Block. *Acta Petrol. Sin.* 20, 1375–1388 (in Chinese with English abstract).
- Hou, K.J., Li, Y.H., Zou, T.R., Qu, X.M., Shi, Y.R., Xie, G.Q., 2007. Laser ablation-MC-ICP-MS technique for Hf isotope microanalysis of zircon and its geological applications. *Acta Petrol. Sin.* 23, 2595–2604 (in Chinese with English abstract).
- Inner Mongolia Nonferrous Metals Geological Exploration Bureau (IMNMGB), 2013. Report of the Dasuji Mo deposit in Zhuozi County, Inner Mongolia (in Chinese).
- Inner Mongolian Autonomous Region Bureau of Geology and Mineral Resource, 1991. Regional Geology of Inner Mongolian Autonomous Region. Geological Publishing House, Beijing, pp. 1–725 (in Chinese with English abstract).
- Irvine, T.H., Baragar, W.R.A., 1971. A guide to the chemical classification of the common volcanic rocks. *Canadian J. Earth Sci.* 8, 523–548.
- Jacobsen, S.B., Wasserburg, G.J., 1980. Sm-Nd isotopic evolution of chondrites. *Earth Planet. Sci. Lett.* 50, 139–155.
- Jahn, B.M., Wu, F.Y., Lo, C.H., Tsai, C.H., 1999. Crust mantle interaction induced by deep subduction of the continental crust: Geochemical and Sr-Nd isotopic evidence from post-collisional mafic-ultramafic intrusions of the Northern Dabie Complex, central China. *Chem. Geol.* 157, 119–146.
- King, P.L., White, A.J.R., Chappell, B.W., Allen, C.M., 1997. Characterization and origin of aluminous A-type granites from the Lachlan fold belt, Southeastern Australia. *J. Petrol.* 38, 371–391.
- Li, C., Qu, W.J., Zhou, L.M., Du, A.D., 2010. Rapid Separation of Osmium by Direct Distillation with Carius Tube. *Rock. Rock. Mineral Anal.* 29, 14–16 (in Chinese with English abstract).
- Li, H.Y., 2012. Analysis on geological characteristics and prospecting indicators of Dasuji molybdenum ore, Inner Mongolia. *Miner. Explor.* 3, 310–318 (in Chinese with English abstract).
- Li, J.Y., 2006. Permian geodynamic setting of Northeast China and adjacent regions: closure of the Paleo-Asian Ocean and subduction of the Paleo-Pacific Plate. *J. Asian Earth Sci.* 26, 207–224.
- Li, X.H., Li, Z.X., Li, W.X., Liu, Y., Yuan, C., Wei, G.J., Qi, C.S., 2017a. U-Pb zircon, geochemical and Sr-Nd-Hf isotopic constraints on age and origin of Jurassic I- and A-type granites from central Guangdong, SE China: a major igneous event in response to foaming of a subducted flat-slab? *Lithos* 96, 186–204.
- Li, J.Y., Gao, L.M., Sun, G.H., Li, Y.P., Wang, Y.B., 2017b. Shuangjingzi Middle Triassic syn-collisional crust-derived granite in the east Inner Mongolia and its constraint on the timing of collision between Siberian and Sino-Korean paleo-plates. *Acta Petrol. Sin.* 33, 565–582 (in Chinese with English abstract).
- Li, D.Y., Nutman, A.P., Compston, W., Wu, J.S., Shen, Q.H., 1992. Remnants of ≥ 3800 Ma crust in the Chinese part of the Sino–Korean craton. *Geology* 20, 339–342.
- Liu, J., Mao, J.W., Wu, G., Wang, F., Luo, D.F., Hu, Y.Q., 2014. Zircon U-Pb and molybdenite Re-Os dating of the Chalkukou porphyry Mo deposit in the northern Great Xing'an Range, China and its geological significance. *J. Asian Earth Sci.* 79, 696–709.
- Liu, J.M., Zhao, Y., Sun, Y.L., Li, D.P., Liu, J., Chen, B.L., Zhang, S.H., Sun, W.D., 2010. Recognition of the latest Permian to Early Triassic Cu–Mo mineralization on the northern margin of the North China block and its geological significance. *Gondwana Res.* 17, 125–134.
- Ludwig, K.R., 2003. Isoplot 3.0—a geochronological toolkit for Microsoft Excel. Berkeley Geochronology Center, Spec. Publ. 4, 70.
- Maniar, P.D., Piccoli, P.M., 1989. Tectonic discrimination of granitoids. *Geol. Soc. Am. Bull.* 101, 635–643.
- Meng, E., Xu, W.L., Yang, D.B., Qiu, K.F., Li, C.H., Zhu, H.T., 2011. Zircon U-Pb chronology, geochemistry of Mesozoic volcanic rocks from the Lingquan basin in Maznholu area, and its tectonics. *Acta Petrologica Sinica* 27 (4), 1209–1226 (in Chinese with English abstract).
- Miao, L.C., Fan, W.M., Liu, D.Y., Zhang, F., Shi, Y., Guo, F., 2008. Geochronology and geochemistry of the Hegenshan ophiolitic complex: implications for late stage tectonic evolution of the Inner Mongolia-Daxinganling Orogenic Belt, China. *J. Asian Earth Sci.* 32, 348–370.
- Nie, F.J., Liu, Y.F., Zhao, Y.A., Cao, Y., 2012. Discovery of Dasuji and Caosiyao large-size Mo deposits in central Inner Mongolia and its geological significances. *Miner. Depos.* 31, 930–940 (in Chinese with English abstract).
- Niu, X.L., Chen, B., Feng, G.Y., Liu, F., Yang, J.S., 2017. Origin of Lamprophyres from the northern margin of the North China Craton: Implications for mantle metasomatism. *J. Geol. Soc.* 174, 353–364.
- Niu, X.L., Chen, B., Liu, A.K., Suzuki, K., Ma, X., 2012. Petrological and Sr-Nd-Os isotopic constraints on the origin of the Fanshan ultrapotassic complex from the North China Craton. *Lithos* 149, 146–158.
- Nowell, G.M., Kempton, P.D., Noble, S.R., Fitton, J.G., Saunders, A.D., Mahoney, J.J., Taylor, R.N., 1998. High precision Hf isotope measurements of MORB and OIB by thermal ionisation mass spectrometry: insights into the depleted mantle. *Chem. Geol.* 149, 211–233.
- Pearce, J.A., Harris, N.B.W., Tindle, A.G., 1984. Trace element discrimination diagrams for the tectonic interpretation of granitic rocks. *J. Petrol.* 25, 956–983.
- Peccerillo, A., Taylor, A.R., 1976. Geochemistry of Eocene calc-alkaline volcanic rocks from the Kastamonu area, Northern Turkey. *Contr. Miner. Petro.* 58, 63–81.
- Qiu, K.F., Deng, J., 2017. Petrogenesis of granitoids in the Dewulu skarn copper deposit: implications for the evolution of the Paleotethys ocean and mineralization in Western Qinling, China. *Ore Geol. Rev.* 90, 1078–1098.
- Qiu, K.F., Li, N., Taylor, R.D., Song, Y.H., Song, K.R., Han, W.Z., Zhang, D.X., 2014. Timing and duration of metallogenesis of the Wenquan deposit in the West Qinling, and its constraint on a proposed classification for porphyry molybdenum deposits. *Acta Petrol. Sin.* 30, 2631–2643 (in Chinese with English abstract).
- Qiu, K.F., Marsh, E., Yu, H.C., Pfaff, K., Gulbransen, C., Gou, Z.Y., Li, N., 2017. Fluid and metal sources of the Wenquan porphyry molybdenum deposit, Western Qinling, NW China. *Ore Geol. Rev.* 86, 459–473.
- Qiu, K.F., Taylor, R.D., Song, Y.H., Yu, H.C., Song, K.R., Li, N., 2016. Geologic and geochemical insights into the formation of the Taiyangshan porphyry copper-molybdenum deposit, Western Qinling Orogenic Belt, China. *Gondwana Res.* 35, 40–58.
- Qiu, K.F., Yu, H.C., Gou, Z.Y., Liang, Z.L., Zhang, J.L., Zhu, R., 2018. Nature and origin of Triassic igneous activity in the Western Qinling Orogen: the Wenquan composite pluton example. *Int. Geol. Rev.* 60, 242–266.
- Santosh, M., Liu, D., Shi, Y., Liu, S.J., 2013. Paleoproterozoic accretionary orogenesis in the North China Craton: a SHRIMP zircon study. *Precambrian Res.* 227, 29–54.
- Santosh, M., Liu, S.J., Tsunogae, T., Li, J.H., 2012. Paleoproterozoic ultrahigh temperature granulites in the North China Craton: implications for tectonic models on extreme crustal metamorphism. *Precambrian Res.* 222–223, 77–106.
- Scherer, E.E., Munker, C., Mezger, K., 2001. Calibration of the Lutetium-Hafnium clock. *Science* 293, 683–687.
- Schiano, P., Monziger, M., Eissen, J.P., Martin, H., Koga, K.T., 2010. Simple mixing as the major control of the evolution of volcanic suites in the Ecuadorian Andes. *Contrib. Mineral. Petr.* 160, 297–312.
- Shao, J.A., Mu, B.L., Zhang, L.Q., 2000. Deep process and shallow response during the tectonic framework translation process in Mesozoic in eastern North China. *Geol. Rev.* 46, 32–40 (in Chinese with English abstract).
- Shu, Q.H., Chang, Z.S., Lai, Y., Zhou, Y.T., Sun, Y., Yan, C., 2016. Regional metallogeny of Mo-bearing deposits in northeastern China, with new Re-Os dates of porphyry Mo deposits in the northern Xilamulun district. *Econ. Geol.* 111, 1783–1798.
- Shu, Q.H., Lai, Y., Wang, C., Xu, J.Y., Sun, Y., 2014. Geochronology, geochemistry and Sr-Nd-Hf isotopes of the Haisugou porphyry Mo deposit, northeast China, and their geological significance. *J. Asian Earth Sci.* 79, 777–791.
- Shu, Q.H., Lai, Y., Zhou, Y.T., Xu, J.J., Wu, H.Y., 2015. Zircon U-Pb geochronology and Sr-Nd-Pb-Hf isotopic constraints on the timing and origin of Mesozoic granitoids

- hosting the Mo deposits in northern Xilamulun district, NE China. *Lithos* 238, 64–75.
- Smoliar, M.I., Walker, R.J., Morgan, J.W., 1996. Re-Os ages of group IIA, IIA, IVA, and IVB iron meteorites. *Science* 271, 1099–1102.
- Sun, J.G., Zhang, Y., Xing, S.W., Zhao, K.Q., Zhang, Z.J., Bai, L.A., Ma, Y.B., Liu, Y.S., 2012. Genetic types, ore-forming age and geodynamic setting of endogenic molybdenum deposits in the eastern edge of Xing-Meng orogenic belt. *Acta Petrol. Sin.* 28, 1317–1332 (in Chinese with English abstract).
- Sun, S.S., McDonough, W.F., 1989. Chemical and isotopic systematics of oceanic basalts: Implications for mantle composition and processes. *Geol. Soc. (Special Publication)* 42, 313–345.
- Sylvester, P.J., 1989. Post-collisional alkaline granites. *J. Petrol.* 97, 261–280.
- Tang, K.D., 1990. Tectonic development of Paleozoic fold belts at the north margin of the Sino-Korean craton. *Tectonics* 9, 249–260.
- Wang, B., Zhou, J.B., Wilde, S.A., Zhang, X.Z., Ren, S.M., 2016b. The timing of final closure along the Changchun-Yanji suture zone: Constraints from detrital zircon U-Pb dating of the Triassic Dajianggang Formation, NE China. *Lithos* 261, 216–231.
- Wang, Q., Zhao, Z.H., Xiong, X.L., 2000. The ascertainment of Late Yanshanian A-type granite in Tongbai-Dabie orogenic belt. *Acta Petrol Mineral.* 297–306 (in Chinese with English abstract).
- Whalen, J.B., Currie, K.L., Chappell, B.W., 1987. A-type granites: geochemical characteristics, discrimination and petrogenesis. *Contrib. Mineral. Petro.* 95, 407–419.
- Wilde, S.A., 2015. Final amalgamation of the Central Asian Orogenic Belt in NE China: Paleo-Asian Ocean closure versus Paleo-Pacific plate subduction—a review of the evidence. *Tectonophysics* 662, 345–362.
- Wu, F.Y., Wilde, S., Zhang, G.L., Sun, D.Y., 2004. Geochronology and Petrogenesis of the Post-orogenic Cu-Ni Sulfide-Bearing Mafic-Ultramafic Complexes in Jilin Province, NE China. *J. Asian Earth Sci.* 23, 781–797.
- Wu, F.Y., Jahn, B.M., Wilde, S., Sun, D.Y., 2000. Phanerozoic crustal growth: U-Pb and Sr-Nd isotopic evidence from the granites in northeastern China. *Tectonophysics* 328, 89–113.
- Wu, F.Y., Yang, Y.H., Xie, L.W., 2006. Hf isotopic compositions of standard zircons and baddeleyites used in U-Pb geochronology. *Chem. Geol.* 231, 105–126.
- Wu, G., Li, X.Z., Xu, L.Q., Wang, G.R., Liu, J., Zhang, T., Quan, Z.X., Wu, H., Li, T.G., Zeng, Q.T., Chen, Y.C., 2017. Age, geochemistry, and Sr-Nd-Hf-Pb isotopes of the Caosiyo porphyry Mo deposit in Inner Mongolia, China. *Ore Geol. Rev.* 81, 706–727.
- Wu, H., 2015. Ore-forming fluid study of the Dasuji porphyry molybdenum deposit in Zhuozi County. Inner Mongolia. *China Univ. Geosci.* 1–86 (in Chinese with English abstract).
- Wu, H.Y., Zhang, L.C., Chen, Z.G., Wan, B., 2008. Geochemistries, tectonic setting and mineralization potentiality of the ore-bearing monzogranite in the Kilitu molybdenum (copper) deposit of Xar moron metallogenic belt. Inner Mongolia. *Acta Petrol. Sin.* 24, 867–878 (in Chinese with English abstract).
- Wu, H.Y., Zhang, L.C., Pirajno, F., Shu, Q.H., Zhang, M., Zhu, M.T., Xiang, P., 2016. The Mesozoic Caosiyo giant porphyry Mo deposit in Inner Mongolia, North China and Paleo-Pacific subduction-related magmatism in the northern North China Craton. *J. Asian Earth Sci.* 127, 281–299.
- Wu, H.Y., Zhang, L.C., Wan, B., Chen, Z.G., Xiang, P., Pirajno, F., Du, A.D., Qu, W.J., 2011. Re-Os and $^{40}\text{Ar}/^{39}\text{Ar}$ ages of the Jiguanshan porphyry Mo deposit, Xilamulun metallogenic belt, NE China, and constraints on mineralization events. *Miner. Deposita* 46, 171–185.
- Wu, M.Q., Tian, B.F., Zhang, D.H., Xu, G.Z., Xu, W.X., Qiu, K.F., 2018. Zircon of the No. 782 deposit from the Great Xing'an Range in NE China: Implications for Nb-REE-Zr mineralization during magmatic-hydrothermal evolution. *Ore Geol. Rev.* <https://doi.org/10.1016/j.oregeorev.2018.09.006>.
- Xiao, W.J., Windley, B.F., Hao, J., Zhai, M.G., 2003. Accretion leading to collision and the Permian Solonker suture, Inner Mongolia, China: termination of the central Asian orogenic belt. *Tectonics* 22, 1069–1089.
- Xin, Y.L., Ren, J.L., Peng, Y.Q., Sun, X.Q., 2011. Ending of the mountain-building movement of Xing'an-Mongolian-Jihei Orogenic Belt in Northeast China: evidence from Late Triassic molasse (geotectonic phase). *Geol. Res.* 20, 413–419 (in Chinese with English abstract).
- Xu, B., Charvet, J., Chen, Y., Zhao, P., Shi, G.Z., 2013a. Middle Paleozoic convergent orogenic belts in western Inner Mongolia (China): framework, kinematics, geochronology and implications for tectonic evolution of the Central Asian Orogenic Belt. *Gondwana Res.* 23, 1342–1364.
- Xu, W.L., Ji, W.Q., Pei, F.P., Meng, E., Yu, Y., Yang, D.B., Zhang, X.Z., 2009. Triassic volcanism in eastern Heilongjiang and Jilin provinces, NE China: chronology, geochemistry, and tectonic implications. *J. Asian Earth Sci.* 34, 392–402.
- Xu, W.L., Wang, F., Pei, F.P., Meng, E., Tang, J., Xu, M.J., Wang, W., 2013b. Mesozoic tectonic regimes and regional ore-forming background in NE China: Constraints from spatial and temporal variations of Mesozoic volcanic rock associations. *Acta Petrol. Sin.* 29, 339–353 (in Chinese with English abstract).
- Yang, J.H., Wu, F.Y., Shao, J., Wilde, S., Xie, L.W., Liu, X.M., 2006. Constraints on the timing of uplift of the Yanshan fold and thrust belt, North China. *Earth Planet. Sci. Lett.* 246, 336–352.
- Yang, L.Q., Deng, J., Dilek, Y., Qiu, K.F., Ji, X.Z., Li, N., Taylor, R.D., Yu, J.Y., 2015a. Structure, Geochronology, and Petrogenesis of the Late Triassic Puziba Granitoid Dikes in the Mianlue Suture Zone, Qinling Orogen, China. *Geol. Soc. Am. Bull.* 117 (12), 1831–1854.
- Yang, L.Q., Deng, J., Qiu, K.F., Ji, X.Z., Santosh, M., Song, K.R., Song, Y.H., Geng, J.Z., Zhang, C., Hua, B., 2015b. Magma mixing and crust–mantle interaction in the Triassic monzogranites of Bikou Terrane, central China: Constraints from petrology, geochemistry, and zircon U-Pb-Hf isotopic systematic. *J. Asian Earth Sci.* 98, 320–341.
- Yang, Q.Y., Santosh, M., 2017. The building of an Archean microcontinent: Evidence from the North China Craton. *Gondwana Res.* 50, 3–37.
- Yu, X.Q., Chen, W., Li, W., 2008. Discovery and prospecting significance of Dasuji porphyry molybdenum deposit, Inner Mongolia. *Geol. Prosp.* 44, 28–37 (in Chinese with English abstract).
- Zeng, Q.D., Yang, J.H., Liu, J.M., Chu, S.X., Duan, X.X., Zhang, Z.L., Zhang, W.Q., Zhang, S., 2012a. Genesis of the Chehugou Mo-bearing granitic complex on the northern margin of the North China Craton: Geochemistry, zircon U-Pb age and Sr-Nd-Pb isotopes. *Geol. Mag.* 149, 753–767.
- Zeng, Q.D., Liu, J.M., Chu, S.X., Wang, Y.B., Sun, Y., Duan, X.X., Zhou, L.L., 2012b. Mesozoic molybdenum deposits in the East Xingmeng orogenic belt, northeast China: characteristics and tectonic setting. *Int. Geol. Rev.* 54, 1843–1869.
- Zeng, Q.D., Liu, J.M., Qin, K.Z., Fan, H.R., Chu, S.X., Wang, Y.B., Zhou, L.L., 2013. Types, characteristics, and time space distribution of molybdenum deposits in China. *Int. Geol. Rev.* 55, 1311–1358.
- Zeng, Q.D., Liu, J.M., Xiao, W.J., Chu, S.X., Wang, Y.B., Duan, X.X., Sun, Y., Zhou, L.L., 2012c. Mineralizing types, geological characteristics and geodynamic background of Triassic molybdenum deposits in the northern and southern margins of North China Craton. *Acta Petrol. Sin.* 28, 357–371 (in Chinese with English abstract).
- Zeng, Q.D., Liu, J.M., Zhang, Z.L., Chen, W.J., Zhang, W.Q., 2011. Geology and geochronology of the Xilamulun molybdenum metallogenic belt in eastern Inner Mongolia. *China Int. J. Earth Sci.* 100, 1791–1809.
- Zhai, M.G., Santosh, M., 2013. Metallogeny of the North China Craton: Link with secular changes in the evolving Earth. *Gondwana Res.* 24, 275–297.
- Zhai, M.G., 2010. Tectonic evolution and metallogenesis of North China Craton. *Miner. Depos.* 29, 24–36 (in Chinese with English abstract).
- Zhai, M.G., Santosh, M., 2011. The early Precambrian odyssey of North China Craton: a synoptic overview. *Gondwana Res.* 20, 6–25.
- Zhang, L.C., Wu, H.Y., Wan, B., Chen, Z.G., 2009a. Ages and geodynamic settings of Xilamulun Mo-Cu metallogenic belt in northern part of the North China Craton. *Gondwana Res.* 16, 243–254.
- Zhang, L.C., Wu, H.Y., Xiang, P., Zhang, X.J., Chen, Z.G., Wan, B., 2010a. Ore-forming processes and mineralization of complex tectonic system during the Mesozoic: A case from Xilamulun Cu-Mo metallogenic belt. *Acta Petrol. Sin.* 26, 1351–1362 (in Chinese with English abstract).
- Zhang, P., Zhao, Y., Kou, L.L., Yang, H.Z., Yang, F.C., 2016a. Zircon U-Pb and molybdenite Re-Os geochronology of copper-molybdenum deposits in southeast Liaoning Province, China. *Int. Geol. Rev.* 58, 1481–1491.
- Zhang, S.H., Zhao, Y., Liu, J.M., Hu, J.M., Song, B., Liu, J., Wu, H., 2010b. Geochronology, geochemistry and tectonic setting of the Late Paleozoic-Early Mesozoic magmatism in the northern margin of the North China Block: A preliminary review. *Acta Petrol. Mineral.* 29, 824–842 (in Chinese with English abstract).
- Zhang, T., Chen, Z.Y., Xu, L.Q., Chen, Z.H., 2009d. The Re-Os dating of molybdenite from the Dasuji molybdenum deposit in Zhuozi county of Inner Mongolia and its geological significance. *Rock Miner. Anal.* 28, 279–282 (in Chinese with English abstract).
- Zhang, Z.Z., Wu, C.Z., Gu, L.X., Feng, H., Zheng, Y.C., Huang, J.H., Li, J., Sun, Y.L., 2009e. Molybdenite Re-Os dating of Xintaimen molybdenum deposit in Yanshan-Liaoning metallogenic belt, North China. *Miner. Depos.* 28, 313–320 (in Chinese with English abstract).
- Zhao, G.C., Zhai, M.G., 2013. Lithotectonic elements of Precambrian basement in the North China Craton: Review and tectonic implications. *Gondwana Res.* 23, 1207–1240.
- Zhao, K.Q., 2016. Research on magmatic-fluid process and ore forming of the Mesozoic porphyry Mo metallogenic system in the Eastern of Xing-Meng orogenic belt. Changchun: Jilin Univ. 1–158 (in Chinese with English abstract).
- Zhao, P., Chen, Y., Xu, B., Faure, M., Shi, G.Z., Choulet, F., 2013. Did the Paleo-Asian Ocean between North China block and Mongolia block exist during the late Paleozoic? First paleo magnetic evidence from central-eastern Inner Mongolia, China. *J. Geophys. Res.-Solid. Earth* 118, 1873–1894.
- Zhao, Y., Chen, B., Zhang, S.H., Liu, J.M., Hu, J.M., Liu, J., Pen, J.L., 2010. Pre-Yanshanian geological events in the northern margin of the North China Craton and its adjacent areas. *Geol. China* 37, 900–915 (in Chinese with English abstract).
- Zheng, Y.F., Xiao, W.J., Zhao, G.C., 2013. Introduction to tectonics of China. *Gondwana Res.* 23, 1189–1206.
- Zhu, Y.S., Yang, J.H., Sun, J.F., Zhang, J.H., Wu, F.Y., 2016. Petrogenesis of coeval silica-saturated and silica-undersaturated alkaline rocks: Mineralogical and geochemical evidence from the Saima alkaline complex, NE China. *J. Asian Earth Sci.* 117, 184–207.
- Zong, K.Q., Klemd, R., Yuan, Y., He, Z.Y., Guo, J.L., Shi, X.L., Liu, Y.S., Hu, Z.C., Zhang, Z.M., 2017. The assembly of Rodinia: The correlation of early Neoproterozoic (ca. 900 Ma) high-grade metamorphism and continental arc formation in the southern Beishan Orogen, southern Central Asian Orogenic Belt (CAOB). *Precambrian Res.* 290, 32–48.